PHYSICAL REVIEW D **96,** 036005 (2017)

Scanning the Earth with solar neutrinos and DUNE

A. N. Ioannisian,[1,2] A. Yu. Smirnov,[3,4] and D. Wyler[5]

[1]*Yerevan Physics Institute, Alikhanian Br. 2, 375036 Yerevan, Armenia*
[2]*Institute for Theoretical Physics and Modeling, 375036 Yerevan, Armenia*
[3]*Max-Planck Institute for Nuclear Physics, Saupfercheckweg 1, D-69117 Heidelberg, Germany*
[4]*ICTP, Strada Costiera 11, 34014 Trieste, Italy*
[5]*Physik Institut, Universität Zürich, Winterthurerstrasse 190, CH-8057 Zürich, Switzerland*

(Received 21 May 2017; published 8 August 2017)

We explore oscillations of the solar ^{8}B neutrinos in the Earth in detail. The relative excess of night ν_e events (the day-night asymmetry) is computed as function of the neutrino energy and the nadir angle η of its trajectory. The finite energy resolution of the detector causes an important attenuation effect, while the layer-like structure of the Earth density leads to an interesting parametric suppression of the oscillations. Different features of the $\eta-$ dependence encode information about the structure (such as density jumps) of the Earth density profile; thus measuring the η distribution allows the scanning of the interior of the Earth. We estimate the sensitivity of the DUNE experiment to such measurements. About 75 neutrino events are expected per day in 40 kt. For high values of Δm^2_{21} and $E_\nu > 11$ MeV, the corresponding D-N asymmetry is about 4% and can be measured with 15% accuracy after 5 years of data taking. The difference of the D-N asymmetry between high and low values of Δm^2_{21} can be measured at the 4σ level. The relative excess of the ν_e signal varies with the nadir angle up to 50%. DUNE may establish the existence of the dip in the $\eta-$ distribution at the $(2–3)\sigma$ level.

DOI: 10.1103/PhysRevD.96.036005

I. INTRODUCTION

The Earth matter effect on solar neutrinos predicted long time ago [1–9] has been succesfully established at more than 3σ level [10,11]. SuperKamiokande (SK) has observed the day-night (D-N) asymmetry of the solar neutrino signal defined as $A^s_{DN} \equiv 2(N_D - N_N)/(N_N + N_D)$, where N_N and N_D are the rates of events detected during night and day. A_{DN} has been determined by the fit of the zenith angle dependence of N_N and N_D integrated over the energy interval (4.5–19.5) MeV. In turn, the rates N_N and N_D as functions of zenith angle (shapes) were computed according to the large mixing angle Mikheyev-Smirnov-Wolfenstein solution for certain values of oscillation parameters. The amplitude of the D-N variations was used as fit parameter. In this way, using the best value from the solar data fit (low value), $\Delta m^2_{21} = 4.8 \times 10^{-5}$ eV^2, the asymmetry

$$A^{s,\mathrm{fit}}_{DN} = -[3.3 \pm 1.0(\mathrm{stat}) \pm 0.5(\mathrm{syst})]\% \qquad (1)$$

has been found from a combination of all series of measurements (SK I-IV).

Assuming that there is no energy and zenith angle dependences of the oscillation effect, SK finds a larger asymmetry: $A^s_{DN} = -[4.2 \pm 1.2(\mathrm{stat}) \pm 0.8(\mathrm{syst})]\%$ (SK I-IV) and $A^s_{DN} = -[4.9 \pm 1.8(\mathrm{stat}) \pm 1.4(\mathrm{syst})]\%$ in SK IV alone with additional statistics [10,11].

Previously, Sudbury Neutrino Observatory measured the neutrino spectra during day and night, indicating a nonzero day-night asymmetry [12,13]. Joint analysis of all solar neutrino data gives about a 4σ evidence of the Earth matter effect [14]. SuperKamiokande also presented the first meaningful measurements of the zenith angle distribution of events.

These results mark the beginning of experimental exploration of the Earth matter effects. Future developments in detection techniques and the construction of large mass detectors with high energy resolution will open up the possibility of detailed study of the solar neutrino oscillations in the Earth. The implications of these studies include tomography (scanning) of interior of the Earth, measurements of the neutrino parameters and searches for new physics beyond the $3\nu-$ paradigm.

In fact, there are some hints of new physics already now: the result (1) has reinforced a tension in determination of Δm^2_{21}. Indeed, the asymmetry (1) is in good agreement with the prediction from large mixing angle Mikheyev-Smirnov-Wolfenstein at low value of Δm^2_{21} which provides consistent description of all solar neutrino data. The asymmetry (1) is about 2σ larger than the asymmetry 1.7% expected for the global fit (high) value of Δm^2_{21} dominated by the KamLAND [15] data. Apart from the large observed D-N asymmetry, also an absence of the "spectral upturn" at low energies indicates a low value of Δm^2_{21} [14]. In the future JUNO [16] will measure Δm^2_{21} with very high precision.

The large DN-asymmetry can be (i) just a statistical fluctuation, (ii) a result of incorrect computation of the expected asymmetry or (iii) due to presence of large (nonstandard) matter effect.

Recall that oscillations of solar neutrinos in the Earth, being oscillations of the mass states, are pure matter effects

proportional to the matter potential V. In the case of standard neutrino interactions, a large V is only possible if the chemical composition is abnormal since the density profile of the Earth is very well known [17–19]. The standard matter effect is determined by the number density of electrons n_e which is related to the total density ρ as $n_e = Y_e\rho/m_N$. Here m_N is the nucleon mass and Y_e is the electron fraction. $Y_e = 1/2$ for an isotopically neutral medium (which is realized in the mantle) and $Y_e = 1$ for Hydrogen. Therefore the required increase of the matter effect is possible if one assumes an abnormally high percentage of hydrogen in the Earth. According to the hydric model of the Earth [20], a large abundance of hydrogen exists in the core of the Earth. However, due to the attenuation effect to be discussed below, SK (having bad reconstruction of the neutrino energy) is not sensitive to the core. So, even this exotic model does not allow us to resolve the tension.

Still another possibility is to assume the existence of nonstandard neutrino interactions [21,22] (see also the review [14]). We do not further elaborate on this.

In anticipation of future experiments, in this paper we study in detail the Earth matter effect on the high energy part of the Boron neutrino spectrum. For previous studies see [23–25] and references therein. (Oscillations of the solar ^{7}Be neutrinos in the Earth have been explored in [26].) Here e compute the nadir angle dependence ($\eta \equiv \pi - \theta_z$, θ_z being the zenith angle) of the relative excess of the night events

$$A_{\rm ND}(\eta, E) \equiv \frac{N_N}{N_D} - 1 \tag{2}$$

for different energies [36]. The distributions $A_{DN}(\eta, E)$ is then integrated over energy, weighted with the energy resolution (reconstruction) function of a detector. We study the dependence of these integrated distributions on the width of the energy resolution function. A complete interpretation of the nadir angle distributions and their dependence on features of the Earth density profile is given. Thus, studies of the nadir angle distribution allow us to scan the density profile of the Earth which is not possible for fixed η [27].

The paper is organized as follows: In Sec. II we summarize the relevant information on oscillations in the Earth. We further develop a theory of neutrino oscillations in a multilayer medium. The results are presented in the full three neutrino framework, see [28] for the constant density case. In Sec. III we compute the relative excess $A_{\rm ND}$ as function of the nadir angle and explore effect of the integration over energy with an energy resolution function of different widths and give an interpretation of the obtained dependences. As an example, in Sec. IV we estimate the ability of the DUNE experiment to measure the Earth matter effects. Conclusions are given in Sec. V.

II. OSCILLATIONS IN THE EARTH

Solar neutrinos arrive at the Earth as incoherent fluxes of the mass eigenstates ν_i. The fractions of these fluxes are determined by the mixing matrix elements in the production region: $P_{\nu_i} = |U^m_{ei}|^2$. In the standard parametrization of the Pontecorvo-Maki-Nakagawa-Sakata mixing matrix they equal

$$P_{\nu_1} = c^2_{13}\cos^2\bar\theta^\odot_{12}, \qquad P_{\nu_2} = c^2_{13}\sin^2\bar\theta^\odot_{12}, \qquad P_{\nu_3} \approx s^2_{13}, \tag{3}$$

where the angle $\bar\theta^\odot_{12}$ is given by

$$\cos 2\bar\theta^\odot_{12} \approx \frac{\cos 2\theta_{12} - c^2_{13}\bar\epsilon_\odot}{\sqrt{(\cos 2\theta_{12} - c^2_{13}\bar\epsilon_\odot)^2 + \sin^2 2\theta_{12}}}. \tag{4}$$

Here the symbol $\odot$ refers to the solar production environment,

$$\epsilon_\odot \equiv \frac{2V_\odot E}{\Delta m^2_{21}}, \tag{5}$$

$c_{13} \equiv \cos\theta_{13}$, $s_{13} \equiv \sin\theta_{13}$. At low (solar neutrino) energies the matter effect on 1-3 mixing can be neglected, so that $\bar\theta^\odot_{13} \approx \theta_{13} = 8.4°$ [29]. Bars at θ's and ϵ mean averaging over the density in the ^{8}B neutrino production region.

In the Earth each mass state splits into eigenstates in matter and oscillates. Then the probability to find ν_e in the detector equals

$$P = \sum_i P_{\nu_i} P_{ie} = \sum_i |U^\odot_{ei}|^2 P_{ie},$$

where P_{ie} is the probability of $\nu_i \to \nu_e$ transition in the Earth. The probability P can be rewritten as

$$P = c^2_{13}(\cos 2\bar\theta^\odot_{12} P_{1e} + c^2_{13}\sin^2\bar\theta^\odot_{12}) + s^4_{13}, \tag{6}$$

where we used the unitarity relation: $P_{1e} + P_{2e} + s^2_{13} = 1$ or $P_{2e} = c^2_{13} - P_{1e}$. Oscillations of ν_3 are neglected.

In the Earth oscillations proceed in the low density regime when $\epsilon_m \ll 1$: at $E \sim 10$ MeV and surface density we have $\epsilon_m \sim 0.03$. Here, $\epsilon_m(x)$ is defined as in Eq. (5), but with the potential V_e taken in the Earth at position x; a super(sub)script m indicates that the respective quantity has to be taken inside the Earth matter. Consequently, the oscillation length in matter

$$l_m = \frac{2\pi}{\Delta^m_{21}(x)} = l_\nu[1 + \cos 2\theta_{12} c^2_{13}\epsilon_m(x) + O(\epsilon^2_m)], \tag{7}$$

is rather close to the vacuum oscillation length

$$l_m \approx l_\nu \approx 330 \text{ km}\left(\frac{7.5\times 10^{-5}\text{ eV}^2}{\Delta m^2_{21}}\right)\left(\frac{E}{10\text{ MeV}}\right).$$

In Eq. (7)

$$\Delta^m_{21}(x) \equiv \frac{\Delta m^2_{21}}{2E}\sqrt{[\cos 2\theta_{12} - c^2_{13}\epsilon_m(x)]^2 + \sin^2 2\theta_{12}} \quad (8)$$

is the splitting of the eigenvalues in matter at position x.

During day, $P_{1e} = P^0_{1e} = c^2_{13}\cos^2\theta_{12}$ and Eq. (6) gives

$$P_D = \frac{c^4_{13}}{2}(1 + \cos 2\bar{\theta}^\odot_{12}\cos 2\theta_{12}) + s^4_{13}. \quad (9)$$

Then the total probability P can be represented as

$$P \equiv P_D + \Delta P, \quad (10)$$

where

$$\Delta P = c^2_{13}\cos 2\bar{\theta}^\odot_{12}(P_{1e} - P^0_{1e}) \quad (11)$$

describes the Earth matter effect.

The probability of the $\nu_1 \to \nu_e$ transition in the Earth, P_{1e}, is determined by dynamics of the 2ν- subsystem in the propagation basis after decoupling of the third state (see for details, e.g., [28,14]). The propagation basis ν' is related to the original flavor basis ν_f, in particular, by the 1-3 rotation $U_{13}(-\theta_{13})$. The Hamiltonian of the 2ν subsystem is characterized by the mixing angle θ_{12}, the mass squared difference Δm^2_{21} and the potential $c^2_{13}V_e$.

The following derivation of P_{1e} reflects immediately the features of the density profile of the Earth which can be considered as a multilayer medium with slowly varying density inside the layers and sharp density changes (jumps) at the borders between the layers. Within the layers, due to slow density change the neutrinos evolve adiabatically, that is, the transitions between the eigenstates are absent, and they evolve independently. Indeed, departure from the adiabaticity is quantified by the parameter γ,

$$\gamma \equiv \frac{1}{\Delta^m_{21}}\frac{d\theta^m_{12}}{dx} \approx \frac{\epsilon_m}{2\pi}\frac{l_m}{h_E}, \quad (12)$$

where $h_E \equiv V/(dV/dx)$ is the scale of the density change within the layers. The second equality in (12) follows from Eqs. (4) and (5) with $\bar{\epsilon}_\odot$ substituted by ϵ_m. θ^m_{12} is the mixing angle in matter. To get an estimate of γ we take $h_E = R_E$, where R_E is the radius of the Earth, and a typical oscillation length $l_m \approx l_\nu \approx 420$ km (for $E = 12.5$ MeV). This gives $\gamma = 1.6\times 10^{-4}$, so that corrections to the adiabatic result are below 0.02%.

At the borders of the layers, the adiabaticity in strongly (maximally) broken, which corresponds to a sudden change of the basis of eigenstates. Therefore after passing the border a different, coherent mixture of eigenstates emerges.

Within the layer the mixing angle θ^m_{12} changes slowly according to the density change. We will denote the values of the angle in the in the kth layer at its beginning and its end (along the neutrino trajectory) by $\theta^{m,i}_{12,k}$ and $\theta^{m,f}_{12,k}$.

The transition matrix between the initial mass states and final flavor states of the propagation basis, $\nu_i \to \nu'_\alpha$ in such a multilayer medium can be written as

$$S = U^m_n \Pi_{k=n,\ldots 1} D_k U_{k,k-1}. \quad (13)$$

Here n is the number of layers, $U^m_n = U(\theta^m_{12,n}, f)$ is the flavor mixing matrix in the last layer just before a detector (it projects an evolved neutrino state onto the flavor states), $\theta^m_{12,n}$ is the flavor mixing angle in the n-layer. The matrix of basis change between the $(k-1)$th and kth layers

$$U_{k,k-1} = U_{k,k-1}(-\Delta\theta_{k-1}), \quad (14)$$

is the matrix of rotation on the angle $\Delta\theta_{k-1}$, where

$$\Delta\theta_{k-1} \equiv \theta^{m,i}_{12,k} - \theta^{m,f}_{12,k-1} \quad (15)$$

is the difference of mixing angles in matter after the $(k-1)$ th jump, i.e., in the beginning of the layer k and before the jump, i.e., at the end of the layer $k-1$. Finally, D_k is the adiabatic evolution matrix of eigenstates in the layer k:

$$D_k = \text{diag}(e^{-i\phi^m_k/2}, e^{i\phi^m_k/2}), \quad (16)$$

where ϕ_k is the adiabatic phase acquired in the layer k

$$\phi^m_k(E) \equiv \int_{x_{k-1}}^{x_k} dx\Delta^m_{21}(x). \quad (17)$$

The diagonal character of D_k reflects the adiabaticity of the neutrino propagation within the layers.

The change of mixing angle in the jump j (15) can be expressed in terms of change of the potential ΔV_j in the layer j as

$$\sin\Delta\theta_j \approx \Delta\theta_j \approx c^2_{13}\sin 2\theta_{12}\frac{E}{\Delta m^2_{21}}\Delta V_j \quad (18)$$

in lowest order in ϵ_m.

The probability of the $\nu_1 \to \nu_e$ transition equals

$$P_{1e} = c^2_{13}|S_{e1}|^2, \quad (19)$$

where the factor c^2_{13} follows from projecting back to the flavor basis: $\nu' \to \nu_f$.

Let us compute the probability in the lowest order in ϵ_m. Since $\Delta\theta_{k-1} \sim \epsilon_m$, the matrix of the basis change can written in the lowest order as

$$U_{k,k-1} \approx I - i\sigma_2 \sin\Delta\theta_{k-1}, \tag{20}$$

where σ_2 is the Pauli matrix. Inserting this expression into (13) and keeping only terms up to order ϵ, we obtain

$$S = U_n^m(\theta_{12,n}^m)\left[D(\phi_{\rm tot}) - i\sum_{j=0}^{n-1}\sin\Delta\theta_j D(\phi_j^a)\sigma_2 D(\phi_j^b)\right], \tag{21}$$

where we introduced summation over the jumps. Here D are diagonal matrices of the form (16) with the total phase acquired in the Earth:

$$\phi_{\rm tot} = \sum_{k=1}^{n}\phi_k, \tag{22}$$

and with the total phases acquired before and after jump j respectively:

$$\phi_j^b = \sum_{k=1}^{j}\phi_k, \qquad \phi_j^a = \sum_{k=j+1}^{n}\phi_k. \tag{23}$$

Using (21) we find explicitly the $e1$- element:

$$|S_{e1}| = \left|\cos\theta_{12,n}^{m,f} + \sin\theta_{12,n}^{mf}\sum_{j=0}^{n-1}\sin\Delta\theta_j e^{-i\phi_j^a}\right|, \tag{24}$$

where we have taken into account that $\phi_{\rm tot} = \phi_j^b + \phi_j^a$. The total amplitude (24) can be viewed as a superposition of waves emanating at the jumps. The amplitudes of the waves are determined by the sizes and signs of jumps, so that the sign is positive (negative) if the potential increases (decreases) on the way of neutrinos.

Finally, the probability equals

$$P_{1e} = c_{13}^2\left[(\cos\theta_{12,n}^{m,f})^2 + \sin 2\theta_{12,n}^{m,f}\sum_{j=0}^{n-1}\sin\Delta\theta_j\cos\phi_j^a\right]. \tag{25}$$

According to (24) and (25), the probability is given by the zero order term and the sum of the contributions of the density jumps. The contribution from the individual jumps is given by the sine of change of the mixing angle in a jump (which is $\sim\epsilon_m$), and by the phase factor with the total phase acquired over the distance from a given jump to a detector (see also [30]).

We will use these expressions for interpreting the results of numerical computations in Sec. III.

In Refs. [23,25] the probability P_{1e} has been obtained in more general integral form which describes both jumps effects and adiabatic propagation:

$$P_{1e} = c_{13}^2\cos^2\theta_{12} - \frac{1}{2}\sin^2 2\theta_{12}c_{13}^4\int_0^L dx V_e(x)\sin\phi_{x\to L}^m, \tag{26}$$

where

$$\phi_{x\to L}^m(E) \equiv \int_x^L dx\Delta_{21}^m(x), \tag{27}$$

is the adiabatic phase acquired from a given point of trajectory x to a detector at L. $L = 2R_E\cos\eta$ is the total length of trajectory, and η is its nadir angle. This form is useful for derivation of the attenuation effect (see below).

For the potential $V_e(x)$ with jumps the integration in (26) can be performed explicitly which reproduces the result (25). The phases (27) $\phi_{x_j\to L}^m$, where x_j is the coordinate of jth jump, coincide with ϕ_j^a.

The solar mixing parameter $\cos 2\bar{\theta}_{12}^{\odot}$ can be expressed in terms of P_D using Eq. (9). Then the difference of probabilities (11) becomes

$$\Delta P(E,L) = c_{13}^2(0.5c_{13}^4 + s_{13}^4 - P_D) \times\frac{\sin^2 2\theta_{12}}{\cos 2\theta_{12}}\int_0^L dx V_e(x)\sin\phi_{x\to L}^m. \tag{28}$$

A key element for understanding oscillations in the Earth is the *attenuation effect* [23] which is a consequence of integrating ΔP with the neutrino energy reconstruction function $g(E_r, E)$ over the neutrino energy:

$$\Delta\bar{P}(E_r) = \int dE g(E_r,E)\Delta P(E). \tag{29}$$

E_r is the reconstructed energy of the neutrino. The function $g(E_r, E)$ is determined by the following factors: (i) energy resolution of the detector, (ii) kinematics of reaction, (iii) energy spectrum of produced neutrinos. To see the effect of attenuation, we insert (28) into (29) and have

$$\Delta\bar{P} = c_{13}^2(0.5c_{13}^4 + s_{13}^4 - P_D) \times\frac{\sin^2 2\theta_{12}}{\cos 2\theta_{12}}\int_0^L dx V(x)F(L-x)\sin\phi_{x\to L}^m, \tag{30}$$

which defines an attenuation factor $F(d)$ [23], with $d \equiv L - x$ being the distance from the location of interest to a detector. In (30) the expression in parentheses has been put out of the integral because it depends only weakly on energy. For the Gaussian energy resolution function

$$g(E_r,E) = \frac{1}{\sigma_E\sqrt{2\pi}}e^{-\frac{(E_r-E)^2}{2\sigma_E^2}} \tag{31}$$

we obtain

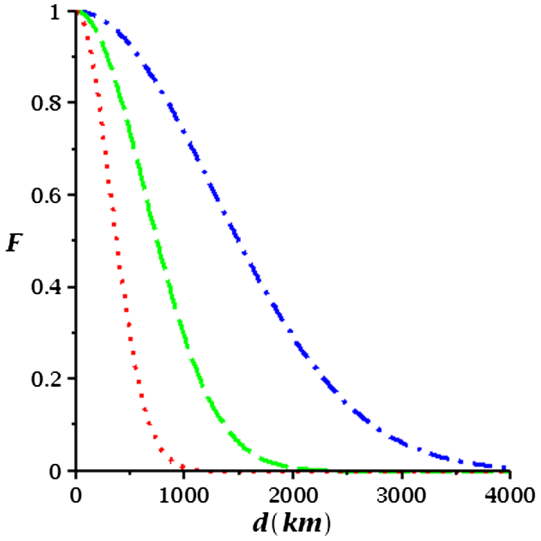

FIG. 1. The attenuation factor F as function of distance from a detector, d, for $E = 11$ MeV and different values of the energy resolution σ_E: 0.5 MeV (blue line), 1 MeV (green line), 2 MeV (red line). We take $\Delta m^2_{21} = 7.5 \times 10^{-5}$ eV^2.

$$F(d) \simeq e^{-2(\frac{d}{\lambda_{\rm att}})^2},$$

where

$$\lambda_{\rm att} \equiv l_\nu \frac{E}{\pi \sigma_E} \tag{32}$$

is the attenuation length. For $d = \lambda_{\rm att}$, the suppression factor equals $F(d) = e^{-2} = 0.135$, and according to (30), the oscillatory effect of structures with $d > \lambda_{\rm att}$ is strongly suppressed. As follows from (32), the better the energy resolution of the detector, the more remote structures can be "seen".

In Fig. 1 we show the attenuation factor for different values of energy resolution. If $\sigma_E/E = 0.1$ and $l_\nu =$ 400 km the attenuation length equals 1470 km and structures of the density profile at $d > 1470$ km can not be seen. For $\sigma_E/E = 0.2$ the structures with $d > 750$ km are strongly attenuated.

III. THE RELATIVE EXCESS OF NIGHT EVENTS

The relative excess of the night events (2) as function of the nadir angle and reconstructed neutrino energy can be written as

$$A_{\rm ND}(E_r, \eta) = \frac{\int dE g(E_r, E) \sigma_{CC}(E) f_B(E) \Delta P(E)}{\int dE g(E_r, E) \sigma_{CC}(E) f_B(E) P_D(E)}. \tag{33}$$

Here $f_B(E)$ is the boron neutrino spectrum [31]. Notice that only 9.7% of ^{8}B neutrinos have energy $E_\nu > 11$ MeV but the corresponding fraction of the detected events is 0.9.

TABLE I. Parameters of the density jumps used in our computations: the depth from the surface, density before a jump, ρ_-, the density after the jump ρ_+, relative size of the jump, nadir angle at which the neutrino trajectory touches the surface of a jump. The eight jumps correspond to the surface of the Earth, the outer crust, the inner crust, lid, low velocity zone, transition zone, low mantle, outer core, inner core.

Jump	depth(km)	$\rho_-(\frac{g}{cm^3})$	$\rho_+(\frac{g}{cm^3})$	$2\frac{\rho_+-\rho_-}{\rho_++\rho_-}$	η_i
J_0^m	0	0	2.60		$\pi/2$
J_1^m	15	2.60	2.90	0.11	1.50
J_2^m	25	2.90	3.38	0.15	1.48
J_3^m	220	3.36	3.44	0.02	1.31
J_4^m	400	3.54	3.72	0.05	1.21
J_5^m	670	3.99	4.38	0.09	1.11
J_1^c	2891	5.57	9.90	0.56	0.577
J_2^c	5150	12.17	12.76	0.05	0.193

We compute the oscillation probabilities $P_D(E)$ and $\Delta P(E)$ according to (6), (9) and (28) using the spherically symmetric model of the Earth with the eight layers parametrization of the PREM density profile [17]. It has 6 density jumps in the mantle J_i^m and 2 density jumps J_j^c in the core. The parameters of the jumps (depth, size, nadir angle of the trajectory which is tangential to the jump) are given in Table I. Trajectories with $\eta < 0.58$ cross the core of the Earth. The change of the solar neutrino flux due to the eccentricity of the Earth orbit ($\pm 3.34\%$) is taken into account.

For the energy resolution function $g(E_r, E)$ we use the Gaussian form (31) with different values of the width σ_E.

For cross sections we take a generic form for interaction with nuclei:

$$\sigma_{CC}(E) = A p_e E_e, \tag{34}$$

where A is a normalization factor (irrelevant for the relative excess), $E_e = E_\nu - \Delta M$, p_e is the electron momentum and ΔM is the threshold of reaction. In computations for DUNE we use $\Delta M = 5.8$ MeV (see below).

Notice that at the energies of Boron neutrinos $\cos 2\tilde{\theta}^\odot_{12} < 0$ and therefore according to (11) the regeneration (increase) of the ν_e flux $\Delta P > 0$ corresponds to suppression of P_{1e}: due to the Earth matter effect $P_{1e} < P^0_{1e}$.

In Fig. 2 we show the relative excess of the night events, $A_{\rm ND}$ (33), as function of the nadir angle and the reconstructed neutrino energy for different values of the energy resolution σ_E. The excess increases with energy. Due to attenuation, remote structures are not seen for poor resolution (bottom panel). In particular, the core of the Earth is not noticeable with $\sigma_E = 2$ MeV, and the dependence on η is as if the core would be absent. With increase of energy, a small oscillatory effect appears due the core at $\eta < 0.58$ since the attenuation is determined by the relative resolution (σ_E/E). Details of the $\eta-$ dependence for different energies

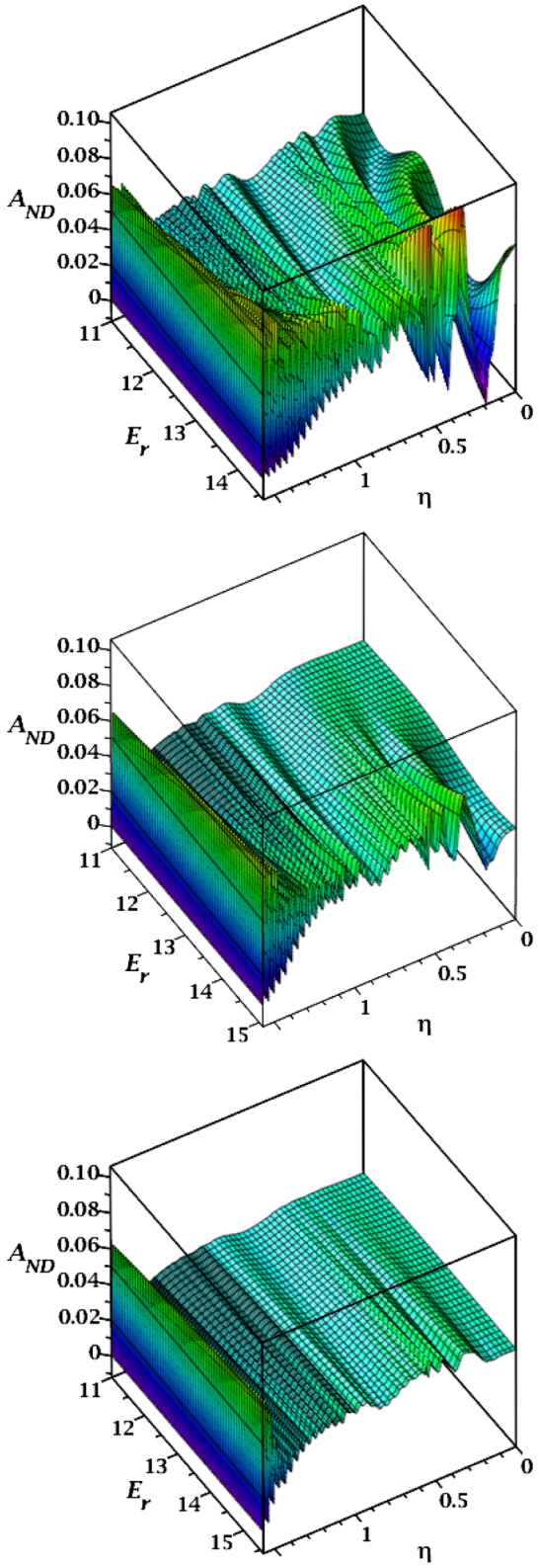

FIG. 2. The relative excess of the night events produced by boron neutrinos as function of the nadir angle and reconstructed neutrino energy for different energy resolutions: $\sigma_E =$ 0.5 MeV (upper panel), 1 MeV (middle panel) and 2 MeV (bottom panel). The Gaussian form of the reconstruction function is used.

can be seen in Fig. 3. Notice that the core of the Earth is clearly visible for $E = 15$ MeV and $\sigma_E = 0.5$ MeV.

Figure 4 (red line) shows the η distribution integrated over the energy above 11 MeV. This integration is equivalent to an energy resolution function of a boxlike form with the average energy 12.5 MeV and energy resolution $\sigma_E = 1.5$ MeV, i.e., $\sigma_E/E = 0.12$. The corresponding attenuation length equals $\lambda_{\rm att} = 1200$ km. The form of the distribution is rather generic. Different computations (including those for SuperKamiokande) give rather similar pattern which can be understood in the following way.

Because of the linearity of the problem, the integration over the energy and the integration of the evolution equation can be permuted. That is, one can first integrate over energy obtaining the attenuation and then consider the flavor evolution, or first, compute the flavor evolution and then perform the energy integration.

Without density jumps ("no-jump" case) the $\eta-$ distribution would have a regular oscillatory pattern with a constant averaged value of $A_{\rm ND}$ determined by the surface density, and the depth of oscillations which decreases with decreasing η (the attenuation effects are stronger for longer trajectories). In the realistic case this (regular oscillatory pattern) occurs only for $\eta > 1.50$ when the neutrino crosses a single outer layer. The period of the oscillatory curve in η, $\Delta\eta$, can be estimated from the condition $\Delta L = 2R_E \sin\eta\Delta\eta = l_m$, which gives

$$\Delta\eta = \frac{l_m}{2R_R \sin\eta}.$$

For $\eta \to 0$ (approaching the core) the period increases. The blue dashed line in Fig. 4 illustrates such a behavior down to $\eta = 0.58$ below which small perturbations appear due to the core effect.

The jumps break adiabaticity and modify the above picture. The deviations start at $\eta = 1.50$, the nadir angle of the neutrino trajectory which touches the surface of the first jump. The length of the trajectory is $L_1 = 875$ km, i.e., approximately $\approx 2l_m$.

Attenuation leads to hierarchy of these jump effects. The jumps J_1^m and J_2^m, closest to a detector, produce the strongest effects (see dotted line in Fig. 4). In turn, jumps J_4^m and J_5^m weakly perturb the picture produced by J_1^m and J_2^m at $\eta < 1.21$ (the density change of J_3^m is too small). Finally, the remote core jumps J_1^c and J_2^c modify the previous picture at $\eta < 0.58$ even more weakly. Let us consider these modifications in order.

As noticed before, the strongest modifications of the "no-jump" picture is produced by the jumps J_1^m and J_2^m at $\eta = 1.4822$ and 1.502 respectively. They suppress the oscillatory behavior at $\eta > 1.45$, produce a dip at $\eta = 1.3$–1.5, and lead to smooth increase of the excess

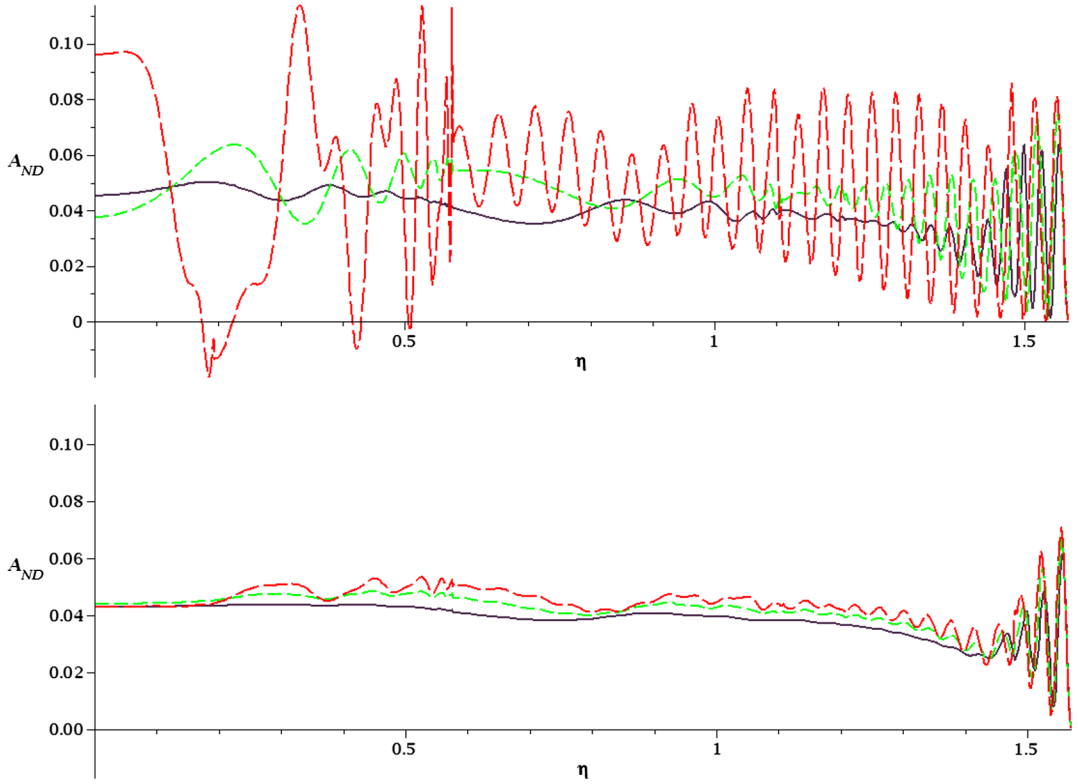

FIG. 3. The relative excess of night events as function of the nadir angle for different values of the reconstructed energy: $E_r = 11$ MeV (violet solid line), 13 MeV (green dash line), and 15 MeV (red long-dash line). The upper (lower) panel corresponds to the energy resolution $\sigma_E = 0.5$ MeV ($\sigma_E = 2$ MeV).

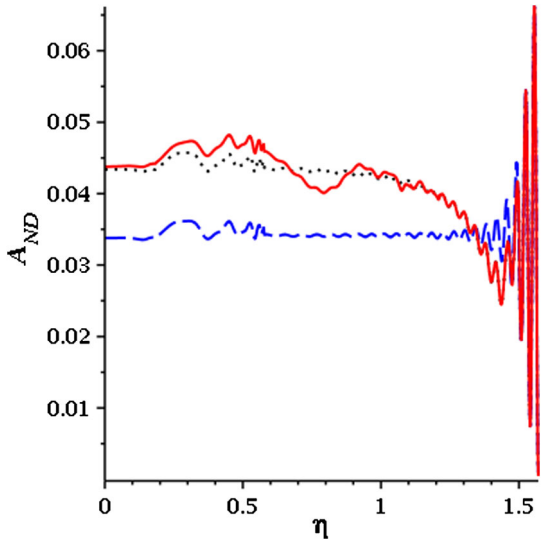

FIG. 4. The relative excess of the night events integrated over $E_r > 11$ MeV as function of the nadir angle of the neutrino trajectory for different density profiles: PREM profile (red solid line); profile without density jumps at 400 and 660 km (black dot line) and with density jumps at outer and inner cores only (blue dash line).

(above no-jump case) with decrease of η. (See dotted line in Fig. 4).

For $\eta > 1.45$ the length of the trajectory is less than the attenuation length; therefore all jumps should be taken into account. For $1.502 > \eta > 1.482$ neutrinos cross three layers and at $\eta < 1.482$—five layers of matter. Furthermore, for the effective energy $E = 12.5$ MeV the oscillation length equals 430 km which is comparable to the lengths of sections of the trajectory in the layers. This leads to a *parametric suppression* of oscillations in addition to averaging: the jumps suppress the third and fourth oscillation maxima in accordance with Fig. 4 (red line). For parametric effects, in general, see [32,33].

To illustrate how it works, let us consider the third maximum of $A_{\rm ND}$ (red line in Fig. 4) at $\eta = 1.489$. For this η the neutrino trajectory crosses three density jumps: $j = 0$, J_0^m at the surface, $j = 1$, $J_1^m(far)$, and $j = 2$, $J_1^m(near)$. This corresponds to crossing three layers: the outer layer twice (at the beginning and the end) and the second one in between. The total length of trajectory is $L \approx 2.5 l_m$, the lengths of the trajectory sections in individual layers equal 238 km, 562 km and 238 km or approximately $0.5 l_m$, $1.5 l_m$ and $0.5 l_m$. Therefore the phases acquired from the three

jumps to a detector equal $\phi_0^m = 5\pi$, $\phi_1^m = 4\pi$ and $\phi_2^m = \pi$. Inserting these numbers into the expression for probability (25) we obtain

$$P_{1e} = c_{13}^2[(\cos\theta_{12,n}^m)^2 + \sin 2\theta_{12,n}^m(-\sin\Delta\theta_0 + \sin\Delta\theta_1 + |\sin\Delta\theta_2|)]. \quad (35)$$

Here the first term in the parenthesis in the second line is the contribution from the jump $j = 0$. Since $\phi_0^m = 5\pi$ and density increases on the way of the neutrinos ($\sin\Delta\theta_0 > 0$), the contribution is negative, thus leading to the positive contribution to the night events excess. The second term, from jump $j = 1$, is positive: now $\phi_0^m = 4\pi$ and the density increases ($\sin\Delta\theta_1 > 0$). The third term (from $j = 2$) is again positive, since $\phi_0^m = \pi$ and density in this jump decreases, so that $\sin\Delta\theta_2 < 0$. Thus, internal jumps suppress the excess (ν_e-regeneration). In other words, the waves "emitted" from the surface jump and the two internal jumps interfere destructively.

The effect can be visualized by an analogy with the electron spin precession in the magnetic field [1,4,33]. In this representation the neutrino state is described by a "polarization vector" $\mathbf{P}$ in flavor space ($\mathbf{x}$, $\mathbf{y}$, $\mathbf{z}$) (see Fig. 5) whose length is $|\mathbf{P}| = 1/2$. The probability to find ν_e in this state is given by the projection of $\mathbf{P}$ on the axis $\mathbf{z}$ (the flavor axis) as $P_e = 0.5 + P_z$. In the layer with a given matter density ρ, $\mathbf{P}$ precesses around the axis $\mathbf{A}$, the direction of eigenstates in this layer. The axis $\mathbf{A}$ lies in the plane ($\mathbf{x} - \mathbf{z}$). The angle between $\mathbf{A}$ and $\mathbf{z}$ is twice the flavor mixing angle in matter, $2\theta_{12}^m$. In vacuum, the angle between the axis of eigenstates (mass eigenstates) $\mathbf{A}_v$ and $\mathbf{z}$ is $2\theta_{12}$. The angle of precession coincides with the oscillation phase. At the borders between layers the mixing angle in matter, and correspondingly, the direction of the axis of eigenstates sharply change.

According to Fig. 5, upper panel a neutrino ν_1 entering the Earth is described by the polarization vector $\mathbf{P}_1$. In the first layer the vector precesses around $\mathbf{A}_1$ by half a period. So, at the border with the second layer it reaches the position $\mathbf{P}_2$. In the second layer the precession proceeds around axis $\mathbf{A}_2$ (whose direction with respect to axis $\mathbf{z}$ is determined by the corresponding mixing angle in matter). The neutrino vector precesses here by 1.5 periods and therefore it enters the third layer in the state $\mathbf{P}_3$. Since the layer 3 has the same properties as the first layer neutrino vector precesses there again by half a period around $\mathbf{A}_1$ and reaches a detector in the state $\mathbf{P}_4$. (Notice that after crossing each layer the opening angle of precession cone systematically decreases.) In the absence of the internal jumps neutrino would be in position $\mathbf{P}_2$. The projection of difference $(\mathbf{P}_4 - \mathbf{P}_2)$ onto the flavor axis $\mathbf{z}$ is positive, thus leading to suppression of the night excess.

This picture can be modified by local density perturbations near the detector. A variation of the depth of the jumps (distance from the surface) can further modify the η dependence leading, e.g., to a parametric enhancement (rather than suppression) of oscillations (see Fig. 6).

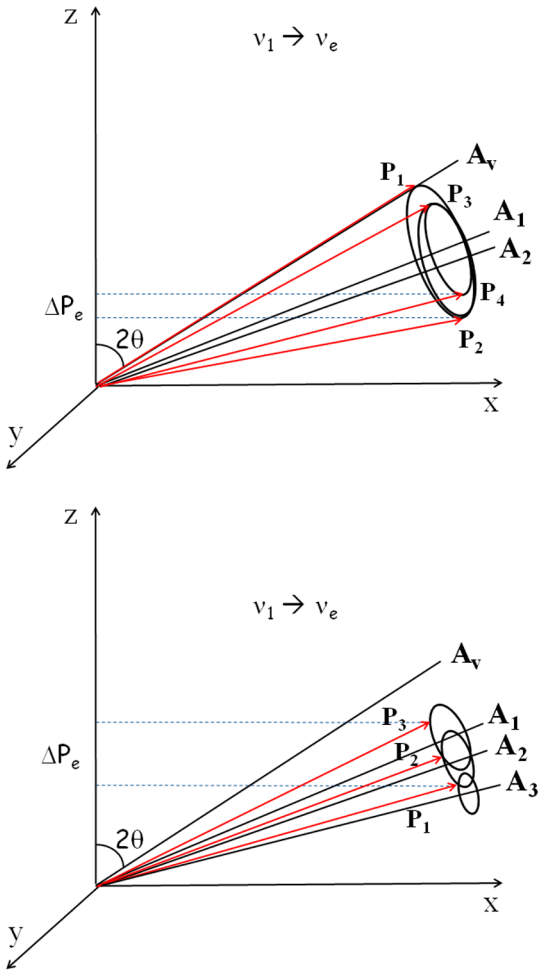

FIG. 5. Graphic representation of the neutrino oscillations in the Earth. Shown are the positions of neutrino polarization vector $\mathbf{P}_i$ at the borders of different layers. $\mathbf{A}_i$ is the precession axis in the layer i. The upper panel: the parametric suppression of oscillations for $\eta = 1.489$; the bottom panel: formation of the dip. See further details in the text.

The dip at $\eta \sim 1.4$ is the interplay of several factors:

(i) In the region of $\eta = (1.20\text{–}1.45)$ after entering the Earth neutrinos cross 4 jumps in the following order: $J_1^m(far)$, $J_2^m(far)$, $J_2^m(near)$, $J_1^m(near)$. Here "far" and "near" determine position of a jump with respect to a detector. At $\eta \sim 1.4$ the length of the trajectory, $L = 2160$ km, is substantially bigger than the attenuation length. Therefore the remote jumps $J_1^m(far)$ and $J_2^m(far)$ (close to the point where neutrinos entered the Earth) are not seen because they are attenuated. Consequently, the effect at a detector is determined by oscillations in the third layer and the jumps closest to a detector $J_2^m(near)$ and $J_1^m(near)$.

(ii) Oscillations in the third layer [between $J_2^m(far)$ and $J_2^m(near)$] are strongly averaged, so the corresponding

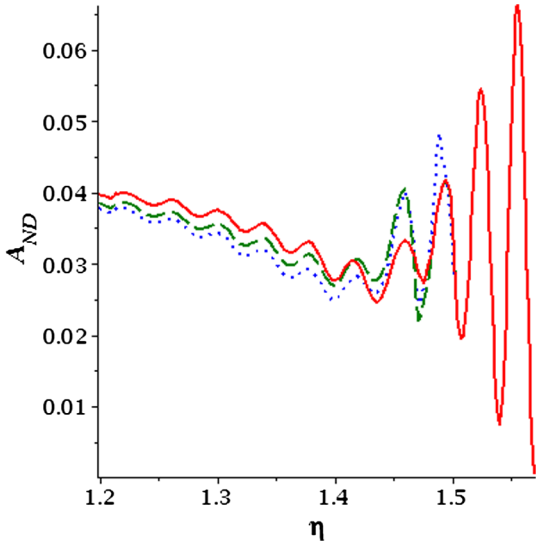

FIG. 6. The relative excess of night events integrated over $E_r > 11$ MeV as function of the nadir angle of the neutrino trajectory for changed parameters for the density jumps. The red line is the conventional one with jumps at 15 km and 25 km; blue-dotted line is for jumps at $h_1 = 20.5$ km and $h_2 = 30$ km; green-dashed line is for jumps at $h_1 = 15$, $h_2 = 30$. Parametric enhancement of oscillations is seen in the 3rd and 4th periods.

oscillation amplitude is effectively small. Thus, the opening angle of the precession cone with respect to axis $\mathbf{A}_3$ in Fig. 5(b) is small. Furthermore, this angle is smaller than the angle between axes A_3 and A_2.

(iii) The length of the trajectory in the outer layers is smaller than $l_\nu/2$ (for $\eta > 1.4$ the length is even smaller than $l_\nu/4$). In this case and also because of (ii) jumps $J_2^m(near)$ and $J_1^m(near)$ with decreasing densities systematically pull the neutrino vector up—to the initial state, i.e., suppressing transition (Fig. 5, bottom panel). After oscillations in the layer 3 around axis $\mathbf{A}_3$ the neutrino vector enters the layer 4 in the state $\mathbf{P}_1$. (Because of smallness of radius of precession similar result will be obtained for any position of $\mathbf{P}_1$ on the precession cone.) It precesses around $\mathbf{A}_2$ ($\equiv\mathbf{A}_4$) by about $1/4$ of the period, from the state $\mathbf{P}_1$ to $\mathbf{P}_2$. In the state $\mathbf{P}_2$ the neutrino enters the layer 5 and precesses around $\mathbf{A}_1$ (which is the same as $\mathbf{A}_5$) by less than $1/4$ of the period. It reaches a detector in the state $\mathbf{P}_3$. The projection of the difference $(\mathbf{P}_4 - \mathbf{P}_1)$ onto the flavor axis is positive implying suppression of the excess.

For $\eta < 1.2$ the lengths of trajectories in the first two layers become much smaller than the oscillation length ($l_i/l_m < 0.1$) and in the first approximation the oscillation effect in these layers can be neglected. In this case one can consider oscillations in the third layer only with initial density as at the border of this layer, that is, $\rho_3 = 3.4$ g/cm^3. Propagation in the layer 3 is adiabatic and therefore the average oscillation effect is determined by its surface density. Consequently, the average oscillation effect here will be bigger than the average effect at the surface by factor ρ_3/ρ_1. This determines the asymptotics of $A_{\rm ND}$ at small η:

$$A_{\rm ND}(\eta = 0) = \frac{\rho_3}{\rho_1} A_{DN}(\eta = 1.57) \tag{36}$$

and $\rho_3/\rho_1 = 1.31$. So, for η below the dip the averaged excess will increase approaching 4.7% as compared to 3.55% at the surface, in agreement with results of computations (Fig. 4).

The pattern produced by J_1^m and J_2^m is further perturbed by the deeper jumps J_4^m and J_5^m. They cause a modulations of the distribution. The jump J_4^m has smaller size than J_5^m, but it is closer to the detector and therefore the two modulations have comparable size. Since J_4^m is closer than J_5^m to a detector, its modulations have a larger period than those of J_5^m for the same range of η. For $\eta \sim 0.8$ the modulations are in phase leading to significant dip. At larger η they are out of phase, reducing the modulations.

The contribution of the core jump J_1^c, in spite of its large size, is strongly attenuated, resulting in even smaller perturbation on the top of those generated by mantle jumps at $\eta < 0.58$.

These qualitative consideration show clearly the sensitive connection between features of the Earth density profile and the η distribution.

IV. PHYSICS REACH OF DUNE

We will assume detection based on the neutrino-nuclei interactions which have several advantages: (i) they have good neutrino energy resolution/reconstruction; (ii) the cross section is much larger than the $\nu e-$ scattering cross section, (iii) the damping factor due to contribution of ν_μ and ν_τ is absent. Correspondingly the asymmetry is enhanced by factor $[1 + \kappa/(P_D(1-\kappa))] \approx 1.6$, where $\kappa \equiv \sigma_{NC}/\sigma_{CC}$ is the ratio of neutral to charged current cross sections of scattering on electrons.

To illustrate the potential of our method, we consider a future DUNE experiment [34]. At DUNE solar neutrinos are detected by the CC process

$$\nu_e + {}^{40}\mathrm{Ar} \xrightarrow{40} \mathrm{K} + e^-. \tag{37}$$

Since ^{40}Ar has spin 0 and the ground state of ^{40}K has spin 4, the transition to the ground state is highly suppressed. The transition(s) via intermediate excited states of ^{40}K (Fermi or Gamov-Teller transitions) with further emission of photons are more probable, although the rates of these transitions are not measured yet.

We approximate the cross section as in (34) with $A \simeq 2 \times 10^{-43}$ cm^2 MeV^{-2}. $\Delta M = 5.8$ MeV is the mass difference between the Fermi exited ^{40}K state and ^{40}Ar. We

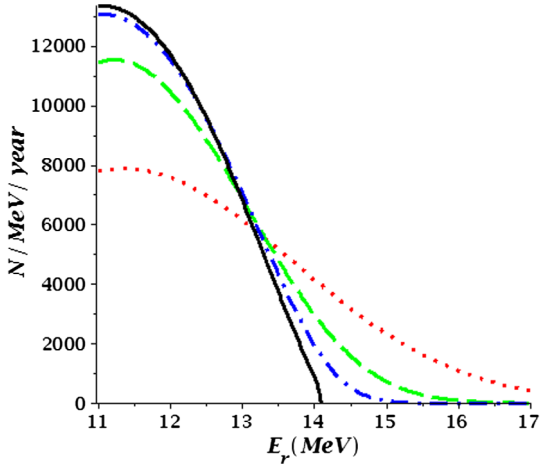

FIG. 7. The energy (E_R) distribution of the annually detected events at DUNE for different energy resolutions σ_E. The solid (black) line represents perfect resolution, $\sigma_E = 0$, the other lines correspond to $\sigma_E = 0.5$ MeV—dash-dotted (blue) line, $\sigma_E = 1$ MeV dashed (green) line, $\sigma_E = 2$ MeV dotted (red) line. The distributions are normalized to annual number of events 27000 at $E_r > 11$ MeV.

consider neutrinos with energy $E_\nu > 11$ MeV, since an electron, to be detected, should have energy above 5 MeV (37).

We find that about 27000 ν_e events will be detected annually for $E_\nu > 11$ MeV in a 40 kt liquid argon detector due to the reaction (37). The energy distribution of these events is shown in Fig. 7. Correspondingly, in 5 years 135000 events will be recorded.

With this statistics the following studies can be performed.

(1) The integral relative excess (Day-Night asymmetry) can be measured with high accuracy. After 5 years of data taking statistical error will be 0.6%. Therefore the average value $A_{\rm ND} = 4\%$ will be measured with 15% accuracy, and its deviation from zero will be established at more than a 6σ level. If $\Delta m^2_{21} = 5 \times 10^{-5}$ eV^2, the average excess equals 6.5% and accuracy of its measurement will be 10% (11σ from 0).

The background is largely unknown, although it is expected that it will have no day-night variations which could mimic or modify the true Earth matter effect. If the signal to background ratio is $S:B = 1:3$, the error bars will be 2 times larger: 1.2%. Consequently, $A_{\rm ND}$ will be measured with 30% accuracy (20% for high values of Δm^2_{21}).

It is straightforward to scale these results with increase of exposure.

(2) Measurements of Δm^2_{21} and search for new physics effects. The difference of $A_{\rm ND}$ between high and low values of Δm^2_{21} is $\Delta A_{\rm ND} = 2.5\%$. After 5 year the difference can be established at 4σ level. If DUNE will confirm the low (solar) value, whereas JUNO will obtain high (KamLAND) value, this will be further evidence of new physics effects, e.g., non-standard neutrino interactions.

(3) Seasonal variations of the flux due to the elliptic orbit of the Earth around the Sun (3.34% amplitude) will be established at $(5\text{–}6)\sigma$ level.

(4) The measurement of the nadir angle distribution of the excess integrated over the energy can be performed with ~30% accuracy (see Fig. 8, upper panel). Here, the exposure function shown in Fig. 9 is important. However, we expect the detection of various structures of the Earth profile will be difficult. The hope is that at least the main feature—the dip and increase of the excess with decrease of η produced by

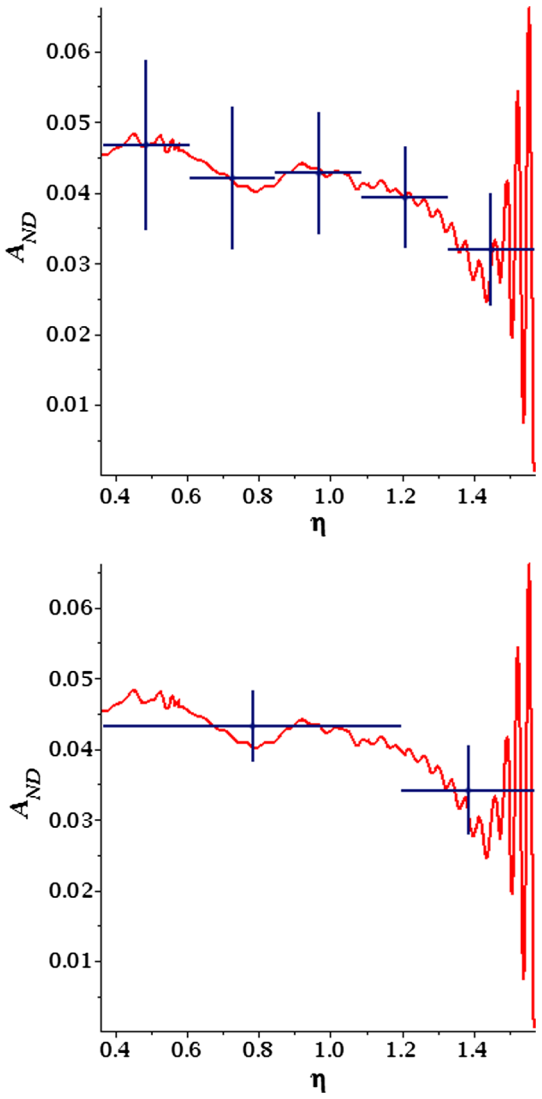

FIG. 8. Scanning of the Earth density profile. The crosses denote the average values of the relative night event excess over the η-interval given by the horizontal line; the vertical lines give the expected accuracy after 5 years of data taking.

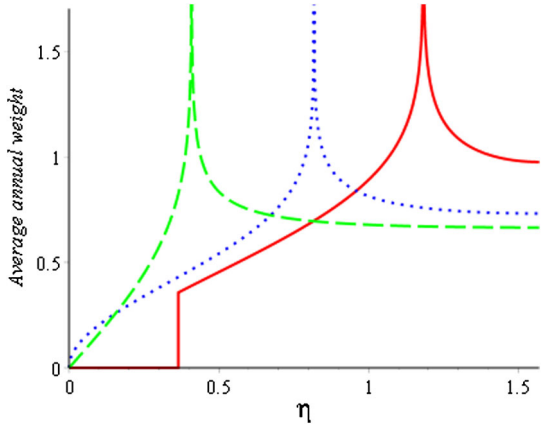

FIG. 9. Annual exposure time as function of nadir angle for different positions of a detector: Homestake mine (red solid line), tropics (dotted blue line), equator (dashed green line).

two closest to surface jumps will be established. In Fig. 8 (bottom panel) we divided the entire interval accessible to DUNE into two bins $\eta = (0.365–1.2)$ and $\eta = (1.2–1.57)$ whose fractions of events are 60% and 40%, respectively. This difference of the numbers of events in the two bins can be established at about 2σ level.

(5) The dependence on energy can be explored; measuring the η-distributions in two, or even more, energy intervals seems feasible.

Measuring the hep neutrino flux will be difficult. Annually, about 130 such neutrinos are expected in the energy interval $14.1 < E_\nu < 18.8$ MeV. Very good energy neutrino reconstruction and high statistics are needed to disentangle them from events produced by the boron neutrinos.

The outer core ($\eta < 0.58$) is "visible" at the Homestake site at about 9% of night time. However, its observation would also require high energy resolution and high statistics.

Another possible realization of ν -nuclei detection is the ASDC-THEIA—future advanced scintillation detector concept which uses water based liquid scintillator (WbLS) [35]. The WbLS can be loaded by metallic ions, in particular ^{7}Li, which will allow to detect the CC process $\nu_e + {}^7\mathrm{Li} \to e + {}^7\mathrm{Be}$.

V. CONCLUSION

(1) In view of forthcoming and planned solar neutrino experiments with large mass detectors and good energy resolution we performed a detailed study of oscillations of the ^{8}B neutrinos in the matter of the Earth. As a model density profile for the earth, we have taken the so called PREM model [17] which approximates the earth by several shells of slowly varying densities. For such a profile we can nicely represent the oscillation amplitude as superposition of the waves emanating from the density jumps between the shells. We have computed the relative excess of the night events (day-night asymmetry) as function of the reconstructed neutrino energy and the nadir angle. Also we have computed the nadir angle distribution of events integrated over the energy above 11 MeV.

(2) The observable distributions are strongly affected by two major effects: Attenuation (due to the finite energy resolution of detectors) and a parametric suppression (or enhancement) of oscillations in the multilayer medium (due to the interplay of wave length and thickness of the layers).

(3) The density jumps influence the distribution substantially. Due to attenuation which affects more contributions from the far away (from the detector) jumps, there is a hierarchy of perturbations determined by the closeness of jumps to a detector. Therefore in a first approximation, the η dependence of the excess is given by the two jumps nearest to the detector.

The η-distribution has the following generic properties:

(a) regular oscillatory pattern for $\eta > 1.502$ (the longer trajectories) with strongly decreased amplitude due to integration over energy.

(b) dip at $\eta = 1.4$ which is due to attenuation of remote jumps and effect of closest jumps where the density decreases when neutrino pass them.

(c) increase of the relative excess with decreasing η below 1.4 and approaching the constant value determined by the density at the borders of third layer.

(d) for $\eta < 1.2$ this first order picture is modulated by smaller effects of two deeper jumps in the mantle.

(e) for $\eta < 0.58$ further perturbations of the above picture show up due to the core of the Earth.

(4) We computed the relative excess of events and its η distribution at DUNE.

After 5 years of data taking DUNE can establish the DN-asymmetry at the 6σ level. The low and high values of Δm^2_{21} can be distinguished at 4σ level.

The first scanning of the Earth matter profile will be possible: The nadir angle distribution can be measured with 30% accuracy. This will allow us to establish the dip in the distribution at 2σ level.

Further developments of the experimental techniques are required to get information about subdominant structures of the η distribution produced by inner mantle jumps and the core.

ACKNOWLEDGEMENTS

A. N. I. thanks the CERN theory department where this work was done for hospitality.

[1] S. P. Mikheyev and A. Yu. Smirnov, Neutrino oscillations in matter with varying density, in *Proc. of the 6th Moriond Workshop on massive Neutrinos in Astrophysics and Particle Physics*, edited by O. Fackler and J. Tran Thanh Van (Tignes, Savoie, France, 1986), p. 355.

[2] E. D. Carlson, Terrestrially enhanced neutrino oscillations, Phys. Rev. D **34**, 1454 (1986).

[3] M. Cribier, W. Hampel, J. Rich, and D. Vignaud, Msw regeneration of solar ν_e in the Earth, Phys. Lett. B **182**, 89 (1986).

[4] J. Bouchez, M. Cribier, J. Rich, M. Spiro, D. Vignaud, and W. Hampel, Matter effects for solar neutrino oscillations, Z. Phys. C **32**, 499 (1986).

[5] S. Hiroi, H. Sakuma, T. Yanagida, and M. Yoshimura, Effects of resonant matter oscillation in Earth on solar neutrino detection, Prog. Theor. Phys. **78**, 1428 (1987).

[6] A. J. Baltz and J. Weneser, Effect of transmission through the Earth on neutrino oscillations, Phys. Rev. D **35**, 528 (1987).

[7] A. Dar, A. Mann, Y. Melina, and D. Zajfman, Neutrino oscillations and the solar neutrino problem, Phys. Rev. D **35**, 3607 (1987).

[8] S. P. Mikheyev and A. Yu. Smirnov, Neutrino oscillations in matter, in *Proc. of 7th Moriond Workshop on Search for New and Exotic Phenomena, Les Arc, Savoie, France, 1987*, edited by O. Fackler and J. Tran Thanh Van (Editions Frontieres, Gif-sur-Yvette, France, 1987), p. 405.

[9] A. J. Baltz and J. Weneser, Matter oscillations: Neutrino transformation in the Sun and regeneration in the Earth, Phys. Rev. D **37**, 3364 (1988).

[10] A. Renshaw *et al.* (Super-Kamiokande Collaboration), First Indication of Terrestrial Matter Effects on Solar Neutrino Oscillation, Phys. Rev. Lett. **112**, 091805 (2014).

[11] K. Abe *et al.* (Super-Kamiokande Collaboration), Solar neutrino measurements in Super-Kamiokande-IV, Phys. Rev. D **94**, 052010 (2016).

[12] Q. R. Ahmad *et al.* (SNO Collaboration), Measurement of Day and Night Neutrino Energy Spectra at SNO and Constraints on Neutrino Mixing Parameters, Phys. Rev. Lett. **89**, 011302 (2002).

[13] B. Aharmim *et al.* (SNO Collaboration), Electron energy spectra, fluxes, and day-night asymmetries of B-8 solar neutrinos from measurements with NaCl dissolved in the heavy-water detector at the Sudbury Neutrino Observatory, Phys. Rev. C **72**, 055502 (2005).

[14] M. Maltoni and A. Y. Smirnov, Solar neutrinos and neutrino physics, Eur. Phys. J. A **52**, 87 (2016).

[15] A. Gando *et al.* (KamLAND Collaboration), Constraints on θ_{13} from a three-flavor oscillation analysis of reactor antineutrinos at KamLAND, Phys. Rev. D **83**, 052002 (2011).

[16] F. An *et al.* (JUNO Collaboration), Neutrino physics with JUNO, J. Phys. G **43**, 030401 (2016).

[17] A. M. Dziewonski and D. L. Anderson, Preliminary reference earth model, Phys. Earth Planet. Inter. **25**, 297 (1981).

[18] P. M. Shearer, in *Upper Mantle Seismic Discontinuities, in Earth's Deep Interior: Mineral Physics and Tomography From the Atomic to the Global Scale*, edited by S.-I. Karato, A. Forte, R. Liebermann, G. Masters, and L. Stixrude (American Geophysical Union, Washington, D. C., 2013).

[19] N. Petersen, L. Vinnik, G. Kosarev, R. Kind, S. Oreshin, and K. Stammler, Sharpness of the mantle discontinuities, Geophys. Res. Lett. **20**, 859 (1993).

[20] L. Bezrukov and V. Sinev, Atmospheric neutrinos for investigation of Earth interior, Phys. Part. Nucl. **47**, 915 (2016).

[21] A. Friedland, C. Lunardini, and C. Pena-Garay, Solar neutrinos as probes of neutrino matter interactions, Phys. Lett. B **594**, 347 (2004).

[22] O. G. Miranda, M. A. Tortola, and J. W. F. Valle, Are solar neutrino oscillations robust?, J. High Energy Phys. 10 (2006) 008.

[23] A. N. Ioannisian and A. Y. Smirnov, Neutrino Oscillations in Low Density Medium, Phys. Rev. Lett. **93**, 241801 (2004).

[24] E. K. Akhmedov, M. A. Tortola, and J. W. F. Valle, A simple analytic three flavor description of the day night effect in the solar neutrino flux, J. High Energy Phys. 05 (2004) 057.

[25] A. N. Ioannisian, N. A. Kazarian, A. Y. Smirnov, and D. Wyler, A precise analytical description of the earth matter effect on oscillations of low energy neutrinos, Phys. Rev. D **71**, 033006 (2005).

[26] A. N. Ioannisian, A. Y. Smirnov, and D. Wyler, Oscillations of the ^{7}Be solar neutrinos inside the Earth, Phys. Rev. D **92**, 013014 (2015).

[27] E. K. Akhmedov, M. A. Tortola, and J. W. F. Valle, Geotomography with solar and supernova neutrinos, J. High Energy Phys. 06 (2005) 053.

[28] M. Blennow, T. Ohlsson, and H. Snellman, Day-night effect in solar neutrino oscillations with three flavors, Phys. Rev. D **69**, 073006 (2004).

[29] F. P. An *et al.* (Daya Bay Collaboration), Measurement of electron antineutrino oscillation based on 1230 days of operation of the Daya Bay experiment, Phys. Rev. D **95**, 072006 (2017).

[30] P. C. de Holanda, W. Liao, and A. Y. Smirnov, Toward precision measurements in solar neutrinos, Nucl. Phys. **B702**, 307 (2004).

[31] J. N. Bahcall, E. Lisi, D. E. Alburger, L. De Braeckeleer, S. J. Freedman, and J. Napolitano, Standard neutrino spectrum from B-8 decay, Phys. Rev. C **54**, 411 (1996).

[32] V. K. Ermilova, V. A. Tsarev, and V. A. Chechin, Kr. Soob. Fiz. [Short Notices of the Lebedev Institute] **5**, 26 (1986); E. K. Akhmedov, Neutrino oscillations in inhomogeneous matter. (In Russian), Yad. Fiz. **47**, 475 (1988) [Sov. J. Nucl. Phys. **47**, 301 (1988)].

[33] P. I. Krastev and A. Y. Smirnov, Parametric effects in neutrino oscillations, Phys. Lett. B **226**, 341 (1989); Q. Y. Liu, S. P. Mikheyev, and A. Y. Smirnov, Parametric resonance in oscillations of atmospheric neutrinos?, Phys. Lett. B **440**, 319 (1998).

[34] R. Acciarri *et al.* (DUNE Collaboration), Long-Baseline Neutrino Facility (LBNF) and Deep Underground Neutrino Experiment (DUNE) conceptual design report volume 2: The physics program for DUNE at LBNF, arXiv:1512.06148.

[35] J. R. Alonso *et al.*, Advanced Scintillator Detector Concept (ASDC): A concept paper on the physics potential of water-based liquid scintillator, arXiv:1409.5864.

[36] This definition differs from the standard D-N asymmetry: $A^s_{DN} = -A_{\rm ND}(1 + 0.5A_{DN})^{-1}$, so the one in (2) is positive and about 2% smaller.